31st Congress of the International Council of the Aeronautical Sciences

Belo Horizonte, Brazil; September 09-14, 2018

# NONLINEAR STATIC AEROELASTIC AND TRIM ANALYSIS OF HIGHLY FLEXIBLE AIRCRAFT

**Zhang Chi*** , **Zhou Zhou*** , **Meng Pu***

*School of Aeronautics, Northwestern Polytechnical University, Xi'an, 710072, PR.China

**Keywords:** *Geometric nonlinearity, Static aeroelasticity, Trim, Stability, All-wing aircraft*

## Abstract

*The static aeroelastic responses, trim solutions and stability analysis of a high aspect-ratio all-wing aircraft without aileron nor rudder is presented. The basics of the computational framework is the coupling of a geometrically nonlinear 3D co-rotational double-spar structural model with a 3D non-planar vortex lattice aerodynamic model. Inertia relief is introduced for the first time to count for the effects of mass distribution on the static deformations of the unconstrained flying aircraft. The aeroelastic deflections, lift distributions, aerodynamic coefficients and their derivatives, as well as the trim solutions and flight dynamic roots are assessed and compared with rigid, linear and nonlinear structural models. Results show that the overall aeroelastic responses, trim solutions and flight dynamic characteristics are highly affected by structural flexibility, revealing the importance of taking into account the geometric nonlinearity in flexible aircraft design and analysis.*

## 1 Introduction

Current studies on high aspect-ratio wings[1, 2] show that geometric nonlinearity plays a dominant role, and the inclusion of geometric nonlinearity is required for accurate aeroelastic predictions, even under normal flight conditions. Many researches[3, 4] give important guidelines and warnings about what to expect in the presence of geometrical nonlinearities and when these become significant in aeroelasticity.

Drela[5] modeled a complete flexible aircraft as an assembly of joined nonlinear beams. Patil et al.[6] and Zhang[7] studied the effects of structural geometric nonlinearities on the aeroelasticity and flight dynamics of HALE aircraft. The geometrically-exact beam theory and ONERA aerodynamic model were used for structural and aerodynamic analyses, respectively. Arena et al.[8] adopted physics-based 3D parametric models of flexible wings based on an exact kinematic approach, giving an improved understanding of the nonlinear phenomena to the dynamic aeroelastic behaviors of flexible wings. Xie et al.[9, 10] investigated the aeroelastic characteristics of a metal single-spar wing under large deformations with nonlinear finite element method (FEM) and the strip theory, 3D lifting line theory and non-planar vortex lattice method (VLM).

In addition, trim analysis and flight stability assessment are essential aspects of aircraft design. Studies by the Department of Aerospace Engineering at the Politecnico di Torino on a solar-powered UAV[11, 12] show that the trim condition and the natural frequencies of flight dynamics could be significantly affected by the inherent flexibility and non-linear deformations of the wing, leading to an overall change in the whole aircraft's aeroelastic performances.

In engineering, a typical wing usually consists of spars, ribs, skin and concentrated mass (engines, propellers, etc.), whose stiffness and mass are not uniformly distributed. However, the commonly used single beam model lacks the capability to incorporate more details of the complex geometries and distributions of mass and

stiffness, which limits their practical usages to some extent.

In this paper, an effective and computationally efficient framework for static aeroelastic trim and stability analysis of flexible subsonic aircraft is presented, where the structural geometric nonlinearity and non-planar effects of the aerodynamic loads are considered. The co-rotational based geometrically nonlinear double-spar FE model is employed for the wing structures. A potential flow based 3D non-planar VLM is considered for its advantages in computational efficiency. The structural and aerodynamic models are tightly coupled by 3D thin plate spline (TPS) method. Inertia relief is introduced for the first time to count for the effects of mass distribution on the static responses of the unconstrained aircraft in flight. The deformed shape and redistributed aerodynamic forces, and nonlinear trim solutions are obtained from a loosely-coupled iteration procedure.

Considering a flexible high aspect-ratio all-wing aircraft, the aeroelastic responses, aerodynamic coefficients and derivatives, trim solutions and flight dynamic roots are obtained and critically compared for rigid, linear and nonlinear structural models. The results give insights into the effects of the structural geometric nonlinearities on the aeroelastic responses, aerodynamic characteristics, trim conditions and flight dynamic characteristics of a complete flexible all-wing aircraft.

## 2 Theoretical Methodologies

### 2.1 Co-rotation based geometrically nonlinear structural model

To capture the large, nonlinear structural deformations of the HALE aircraft, a co-rotational framework is developed based on Euler-Bernoulli beam elements.

In a co-rotational formulation, the rigid-body motions are separated from the strain-producing deformations at the local element level. Herein it is assumed that the 'internal element behavior' is linear whereas nonlinearity are introduced via the co-rotational technique. This is accomplished by attaching an element reference frame to each element and two nodal reference frames to the nodes of each element; these frames translate and rotate with the displacements of the element.

The more detailed descriptions of 3D formulations for a spatial beam and its tangent stiffness matrix, as well as the numerical implementation of the rotational updates and the overall solution strategy can be found in the co-rotational nonlinear finite element literature[13, 14].

### 2.2 Non-planar VLM for aerodynamics

The aerodynamics of deformed lifting surfaces are computed by non-planar VLM, in which the lifting surfaces are deformed with the structure, the boundary condition and the locations of the collocation points are updated according to the deformed configuration of the wing. For more details the reader is referred to[15].

### 2.3 TPS for aerodynamic/structure coupling

As far as load transfer is considered, the thin plate spline (TPS) based on the virtual work principle is chosen. In this way, it is possible to project a force acting on the aerodynamic grid onto the structural one. More thorough treatises on this topic are also shown in[16].

### 2.4 Inertia relief

If a free body is accelerating due to constant unbalanced loads, the inertia relief solution provides the ability to obtain static deflections relative to a set of reference points attached to the moving coordinate system.

The basic equation of inertia relief is

$$\boldsymbol{K}\boldsymbol{u} = \boldsymbol{F} - \boldsymbol{M}\boldsymbol{a} \tag{1}$$

where $\boldsymbol{u}$ is displacements relative to the moving system and $\boldsymbol{a}$ is the steady accelerations to be determined from the mass and loads.

If $\boldsymbol{\Phi}_R$ is a matrix whose columns define the rigid body motions of the structure, then for a freebody,

$$\boldsymbol{\Phi}_R^T\boldsymbol{K}\boldsymbol{u} = \boldsymbol{\Phi}_R^T\boldsymbol{F} - \boldsymbol{\Phi}_R^T\boldsymbol{M}\boldsymbol{a} = \boldsymbol{0} \tag{2}$$

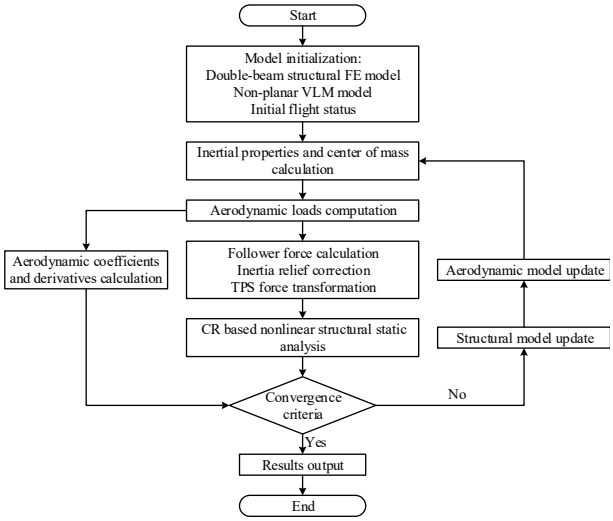


**Fig. 1** Static aeroelastic analysis flow chart

However, since the full-sized vector, $\boldsymbol{a}$, is a rigid body motion, it may be defined in terms of accelerations, $\boldsymbol{a}_R$, by the equation

$$\boldsymbol{a} = \boldsymbol{\Phi}_R \boldsymbol{a}_R \tag{3}$$

Combining Eq.(3) into Eq.(2), we obtain

$$\boldsymbol{a} = \boldsymbol{\Phi}_R \overline{\boldsymbol{M}}^{-1} \boldsymbol{\Phi}_R^T \boldsymbol{F} \tag{4}$$

where the total mass matrix for the reference coordinates is

$$\overline{\boldsymbol{M}} = \boldsymbol{\Phi}_R^T \boldsymbol{M} \boldsymbol{\Phi}_R \tag{5}$$

The resulting equation defined in Eq.(1) may now be arbitrarily constrained since the total load is balanced by the inertia forces.

## 2.5 Aeroelastic model and solution strategy

As illustrated in Fig.1, the nonlinear aeroelastic analysis is conducted by iterative calculations of two modules, the aerodynamic analysis module and the structural static analysis module.

The procedure for the geometrically nonlinear static aeroelastic analysis starts with the appropriate aerodynamic and structural discretization and initialization, followed by the iterative calculations. For each cycle of computation, the aerodynamic model and inertia properties of the whole aircraft are updated according to the latest structural deformations. The external forces are transformed into the structurally equivalent nodal forces by TPS, and then corrected by inertia relief method. The stiffness matrices and structural deformations are updated based on the latest aerodynamic and non-aerodynamic forces. As one cycle finishes, the structural deformations and aerodynamic characteristics will be evaluated and tested for termination. If termination criteria are not met, a new iterative cycle will be excited until a converged solution is found.

**Table 1** Geometrical and structural properties of the all-wing aircraft

| | |
|---|---|
| Wing span | 7.0 m |
| Wing surface area | 3.7 $m^2$ |
| Chord length | 1.2m/0.4m (IW/OW) |
| Dihedral angle | 0°/6° (IW/OW) |
| Incidence angle | 8°/6° (IW/OW) |
| Front spar (IW) | 30%c, 30 mm in diameter |
| Rear spar (IW) | 45%c, 14 mm in diameter |
| Front spar (OW) | 15%c, 24 mm in diameter |
| Rear spar (OW) | 65%c, 14 mm in diameter |
| Young's modulus | 103.7 GPa |
| Poisson's ratio | 0.27 |
| Equivalent density | 9,100 $kg/m^3$ |
| Total mass | 14.7 kg |
| Payload and batteries | 4 kg |

## 3 Modeling of the flexible high aspect-ratio all-wing aircraft

The present model is a flexible high aspect-ratio all-wing aircraft. The inner wing (IW) and outer wing (OW) each has two hollow tubular spars. The wing platform and wing structure are illustrated in Table 1 and Fig.2, respectively.

As with Fig.2, the outer wing each has two spars and 10 equally spaced ribs that are modeled as beam elements to account for their effects on the mass and stiffness distributions of the wing. The properties of the engines and pylons, and batteries and payloads are also accounted for as concentrated mass.

Figure 3 shows the aerodynamic model of the aircraft and there are $28 \times 10$ vortex lattices.

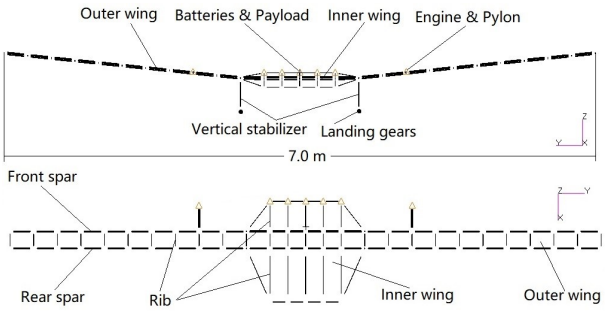


**Fig. 2** Structural finite element model

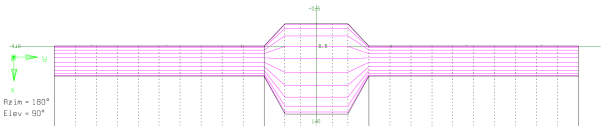

**Fig. 3** Aerodynamic model

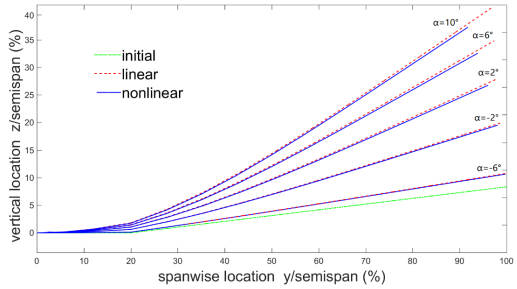


**Fig. 4** Bending deflections of the wings under different angles of attack (H=500m, V=14m/s)

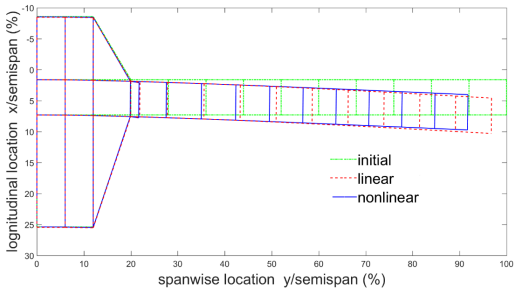


**Fig. 5** Top view of the initial and deformed shape of the all-wing aircraft ($\alpha = 10°$)

## 4 Numerical Results

We now apply our aeroelastic and trim analyses to the flexible aircraft introduced in the previous section. The cruise speed of the aircraft is set to 14 m/s and the altitude is 500 m.

The structural responses of the wing structure are analyzed by the traditional linear model (represented by the label 'linear'), and the proposed co-rotational based geometrically nonlinear model (represented by the label 'nonlinear'), in which geometric nonlinearity effects brought by large deformations are taken into account.

### 4.1 Bending deformations

Fig. 4 shows the variations of the static equilibrium position of the wings, with $\alpha$=-6°, -2°, 2°, 6° and 10°, respectively.

It shows that the vertical displacements of the wings keep increasing as $\alpha$ increases, and the vertical displacement at the wingtip goes to about 40% of the semispan when $\alpha$ is 10°. According to the nonlinear results, the finite-span wing has a large lateral displacement of about 10% of the semispan. This is a typical nonlinear case of a flexible wing with large deformations. While the results attained by the linear model indicate that the vertical displacement of the wingtip goes almost linearly, little lateral displacement occurs.

Figure 5 is the top view of the initial and deformed shape of the right wing, when $\alpha$ is 10°. A lateral displacement in the nonlinear result is evident, which is in accordance with the analysis above. The linear result shows a small lateral displacement, which is caused by the lateral forces introduced by the wing's bending deflections. Comparing the deformed state with the initial one, it can also be seen that, the wing bends upwards and it is accompanied by a backward bending deformation. This phenomenon is frequently seen in high aspect-ratio wings.

### 4.2 Torsional deformations

The torsional deformations of the wings are shown in Fig.6 for selected angles of attack.

It can be seen that a positive torsion occurs

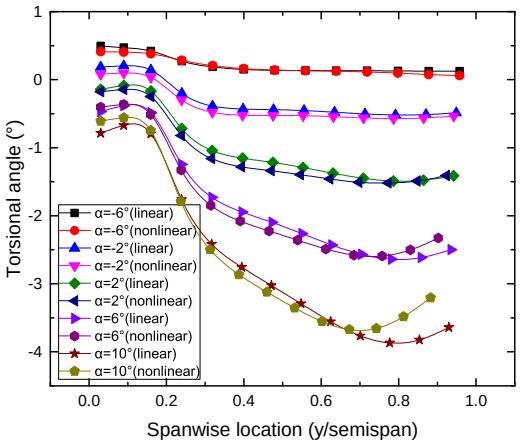


**Fig. 6** Torsional aeroelastic deflections of the wings under different angles of attack

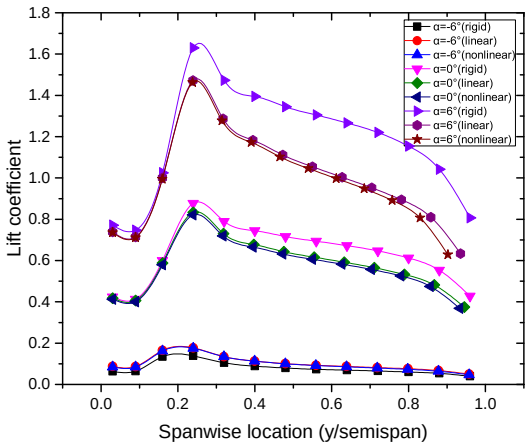


**Fig. 7** Lift coefficient distributions of the wings under different angles of attack

when α is low, while a negative torsion occurs when α is high. This is because the front spar placing at 15% chord has a larger diameter than the rear spar placing at 65%, hence it is much stiffer than the rear one, making the wing's elastic axis lie in front of the aerodynamic center (A.C.) line of the wing. When α is low, the lift on the A.C. is too low to balance the pitch-up moment existing on the A.C., and the nose-up moment brings the positive torsion. When α goes high enough, the lift on the A.C. is high enough to counteract the invariable pitch-up moment. When α increases further, a pitch-down moment arises with the increased lift, bringing the wing's negative torsional deflections. It can be inferred that this kind of structural design and torsional deformation can prevent the static torsional divergence to some extent, but may cause the reversal effects like control reversal.

Besides, the effects of geometrical nonlinearity on the torsional deformations can be inferred from the results obtained by linear and nonlinear models. The torsional deformations obtained by the nonlinear model are larger than that obtained by the linear one.

### 4.3 Spanwise lift distributions

Figure 7 illustrates the spanwise distributions of lift coefficient of the wings, showing that OW have higher lift coefficients than IW. It can also be seen that the flexible wings have higher lift than the rigid one when α is low, and lower lift when α is high, and the flexibility effect increases with the increase of α for both the linear and nonlinear structural models. This is caused by two main reasons, one is that in the present case of large flatwise bending, the aerodynamic forces not act in the vertical direction. The other reason is that the flexible wings undergo negative torsions when α is high, which decreases the local angles of attack, and then the lift drops.

Comparison of linear and nonlinear results show the lift from the nonlinear model is lower than that from the linear one; it agrees with the phenomenon that the nonlinear model produces larger negative torsions.

The initial and final aerodynamic load predictions solved by the nonlinear model, when α is 10°, are illustrated in Fig.8. It can be inferred that the rigid or linear model will give inaccurate results when the structural flexibility is sufficiently high to lead to a large deformation; in this case the nonlinear models can provide more accurate predictions.

### 4.4 Variations of aerodynamic characteristics vs. angle of attack

The variations of aerodynamic coefficients and their derivatives under different angles of attack are calculated using the non-planer VLM coupled

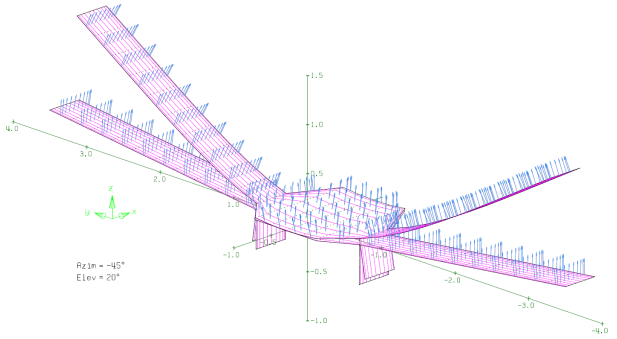

**Fig. 8** Initial and final aerodynamic models of the flexible wing

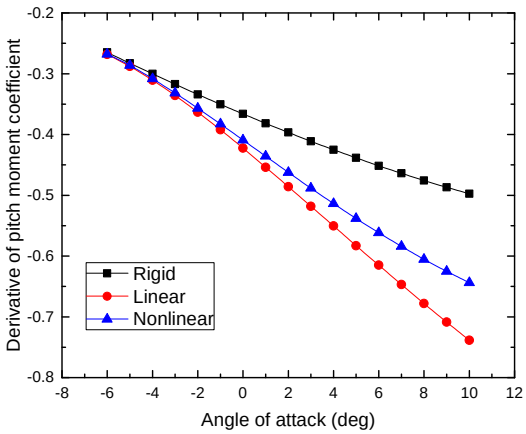


**Fig. 11** Variations of $C_{m_\alpha}$ derivative vs. AOA

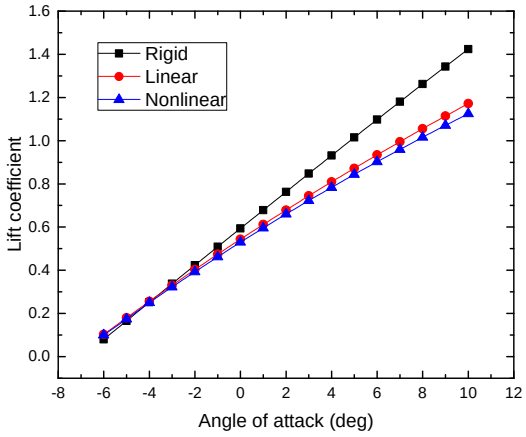


**Fig. 9** Variations of lift coefficient vs. AOA

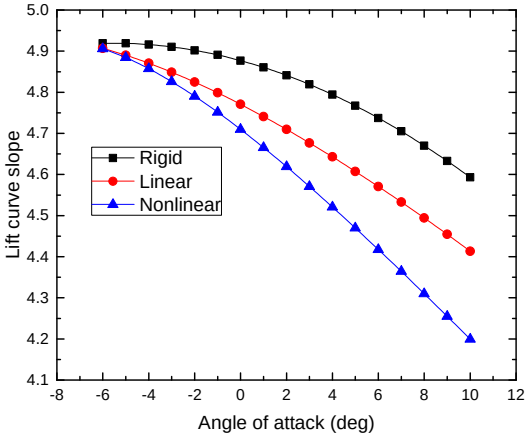


**Fig. 10** Variations of lift curve slope vs. AOA

with linear and nonlinear structural models, and compared with the rigid case, as shown in Fig.9 through Fig.14.

Figure 9 and Fig.10 show that the lift and lift curve slope ($C_{L_\alpha}$) of flexible aircraft are all lower than those of a rigid one, and results from the nonlinear model are even lower than those from the linear one. With α increases, the influence of structural flexibility gets more conspicuous. When α is 10°, the lift coefficients predicted by the linear and nonlinear models are 1.17 and 1.12, which is only 82% and 79% of the lift of the rigid one, while the lift curve slopes drop from 4.59 to 4.41 and 4.19, respectively.

Figure 11 shows the variations of pitch moment coefficient derivative ($C_{m_\alpha}$) obtained by three different structural models. It can be seen that the $C_{m_\alpha}$s of flexible models are much lower than that of the rigid one. The nonlinear model has a smaller absolute value of $C_{m_\alpha}$ than the linear one, and the difference increases with α.

Figure 12 shows the variations of longitudinal static stability margin with α. It can be seen that the stability margin of rigid model increases almost linearly from 5.4% to 10.8% when α increases from -6° to 10°. Linear and nonlinear models show that the stability margin prediction obtained from flexible models is higher than what from the rigid one. The variation and differences among different models is mainly affected by the characteristics of $C_{L_\alpha}$ and $C_{m_\alpha}$.

Under aerodynamic loads, flexible wings un-

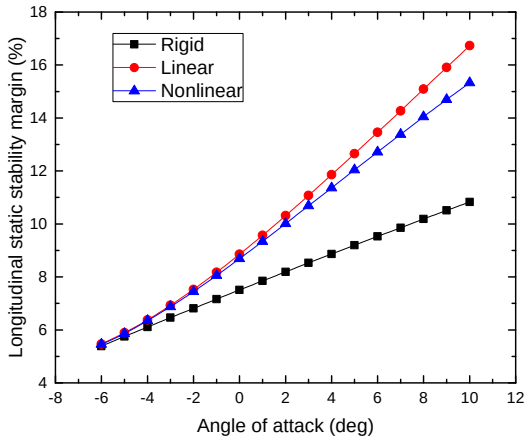


**Fig. 12** Variations of longitudinal static stability margin vs. angle of attack

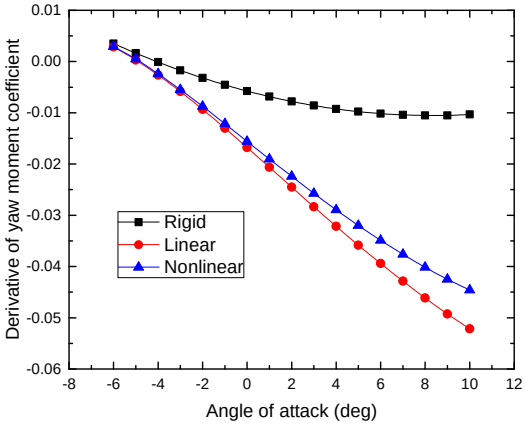


**Fig. 15** Variations of $C_{n_\beta}$ vs. angle of attack

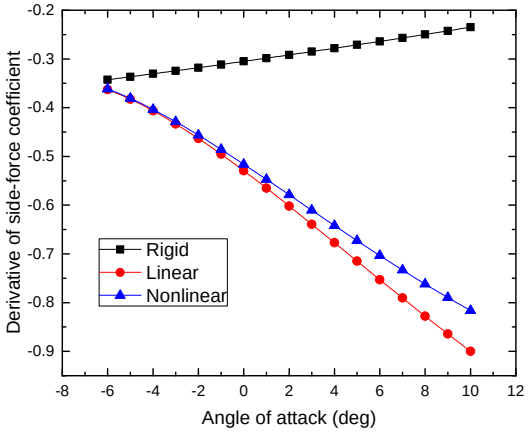


**Fig. 13** Variations of $C_{y_\beta}$ vs. angle of attack

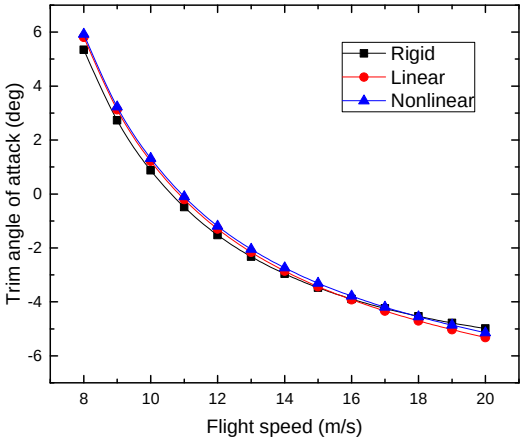


**Fig. 16** Variations of trim AOA with flight speed

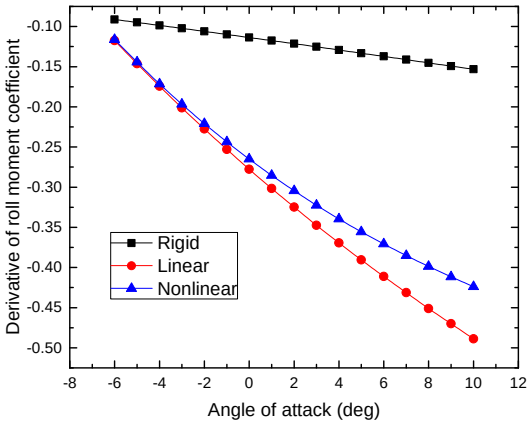


**Fig. 14** Variations of $C_{l_\beta}$ vs. angle of attack

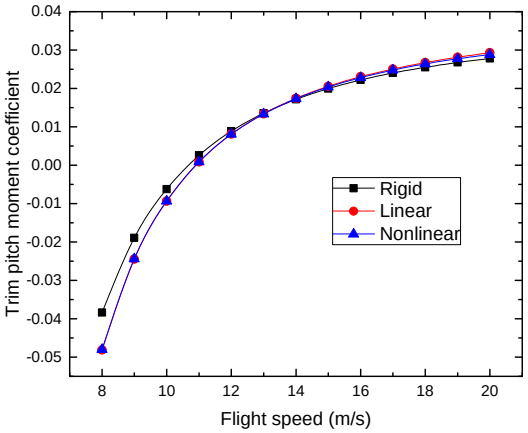


**Fig. 17** Variations of trim $C_m$ with flight speed

dergo large bending deflections, which increases the equivalent angle of dihedral, the latitudinal and directional characteristics of the aircraft will change significantly. The derivatives of side-force, roll moment and yaw moment coefficients at different angles of attack are plotted in Fig.13 through Fig.15, respectively. The side-force derivative $C_{y_\beta}$ is usually negative, and frequently small enough to be neglected entirely, but the absolute values of $C_{y_\beta}$ of both linear and nonlinear models increase with $\alpha$, indicating that the aircraft gets more sensitive to the sideslip when $\alpha$ is large, and so are the trends of $C_{l_\beta}$ and $C_{n_\beta}$. Fig.14 shows that the absolute values of $C_{l_\beta}$ obtained by flexible models increase more rapidly than that of rigid model, which will give rise to larger frequency of Dutch roll.

As for the yaw moment derivative shown in Fig.15, because the vertical stabilizer is too close to the center of gravity, $C_{n_\beta}$ of rigid model is negative but close to zero, showing an approximate neutral weathercock stability, while the $C_{n_\beta}$ of flexible models are negative and decrease with $\alpha$ rapidly, indicating that the weathercock stability is unstable and goes worse with the upward bending deflections.

### 4.5 Trim analysis

The static aeroelastic trim results for the all-wing aircraft is investigated. Here, the trim $\alpha$ is obtained by calculating the angle of attack that gives the required lift.

Figure 16 indicates that the higher flight speed is, the lower trim angle of attack is, and the value of $\alpha$ required from a flexible aircraft is more than that from a rigid one when flight speed is below 16 m/s. This is because the large flatwise bending makes the lifts do not act in the vertical direction. Large deformation and associated loss of aerodynamic force in the vertical direction leads to the requirement of a higher value of $\alpha$, and the value of $\alpha$ required from a nonlinear model is more than that from a linear one.

When the flight speed is above 16 m/s, the trim angles of attack from the flexible models are lower than that from the rigid model, which is caused by the positive torsional aeroelastic deformations when $\alpha$ is low.

The main significance of this result lies in that different models will give different stall speeds. The improper use of a model to predict the performance of a highly flexible aircraft may lead to inaccurate estimations of the flight envelope.

Figure 17 shows that the pitch moment in trim flight increases with flight speed. There is a pitch-down moment when the speed is below 11 m/s, above witch a nose-up moment occurs. Besides, the absolute values of pitch moment in trim obtained from flexible models are larger than that from the rigid one. This result indicates that structural flexibility has effect on pitch moment in trim flight, and the differences of pitch moment will have momentous effects on the design of elevators and longitudinal control laws.

Figure 18 shows that with an increase in flight speed, the longitudinal static stability margin of the aircraft decreases, and is affected by structural flexibility. The stability margin of flexible aircraft is more sensitive than that of a rigid one. The stability margin of flexible models drops from 11.4% to 5.8%, while it decreases merely from 9.3% to 5.7% in rigid case, with the speed increases from 8 m/s to 20 m/s, respectively.

### 4.6 Flight Stability Analysis

When flexibility effects are taken into account in flight dynamic analysis, the performances of a flexible aircraft are distinctly different from those of a rigid one.

Fig. 19 compares the flight dynamic roots obtained with different structural models. The roots at a flight speed of 14 m/s are shown in Table 2.

Results show that the phugoid mode of the aircraft is unstable, and with flight speed increases, the spiral mode goes from stable to unstable.

The longitudinal and latitudinal modes are affected by wing flexibility. Since the large bending deflection of the wing increases the aircraft's moment of inertia about the pitch axis, the damping of short period increases for the flexible models, and the frequency decreases.

As for the latitudinal and directional modes,

**Table 2** Eigen roots of different structural models (V=14m/s)

| Mode | Rigid | Linear | Nonlinear |
|---|---|---|---|
| Phugoid | 0.050±1.005i | 0.066±1.007i | 0.062±1.006i |
| Short Period | -7.688±6.159i | -6.975±5.100i | -6.948±5.118i |
| Dutch | -0.3190±0.860i | -0.2794±1.099i | -0.2769±1.105i |
| Spiral | -0.02573 | -0.06908 | -0.07001 |
| Roll | -12.88 | -13.09 | -12.95 |

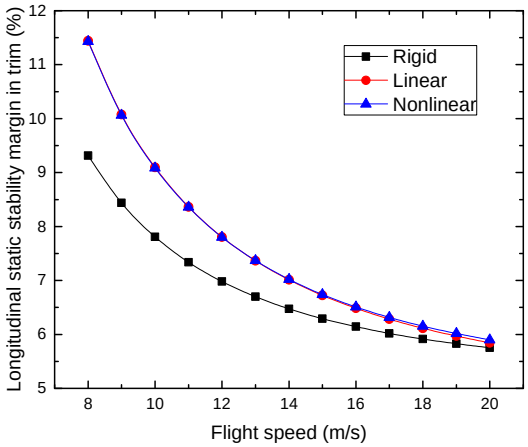


**Fig. 18** Longitudinal stability margin vs. flight speed

due to the wing's large bending deflections, the equivalent angle of dihedral increases, which makes $C_{l_\beta}$ increase, and leads to larger frequency and smaller damping of Dutch mode. The spiral and roll modes of flexible models become more stable than the rigid one.

## 5 Concluding Remarks

Numerical simulations of the static aeroelastic deformations and lift distributions, along with the aerodynamic coefficients and their derivatives, as well as the trim and flight stability solutions of a flexible high aspect-ratio all-wing aircraft are presented. Comparisons for rigid, linear and nonlinear structural models are also supplied.

Results show that the overall characteristics and trim solutions are significantly affected by structural flexibility. Neglecting structural nonlinearities can lead to very different predictions of the aeroelastic behaviors of a flexible aircraft, which might be inaccurate and un-conservative.

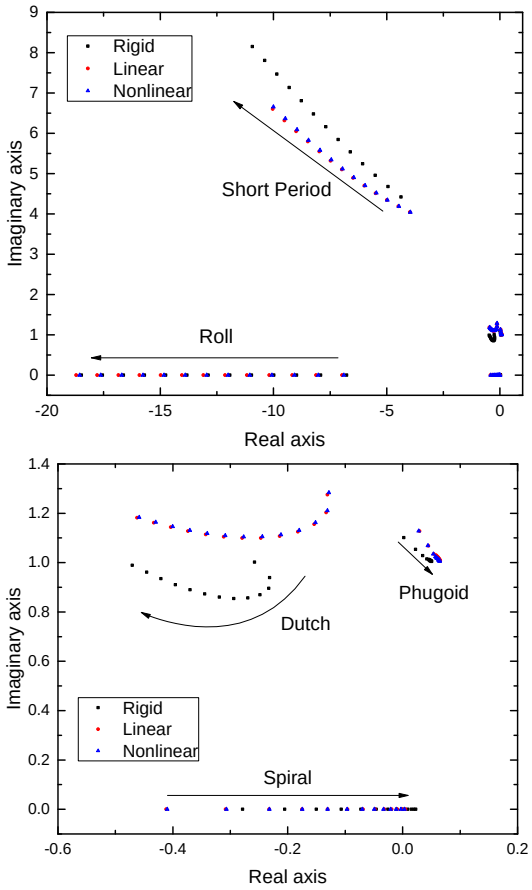


**Fig. 19** Loci of the flight dynamic roots with an increasing flight speed

## References


[1] F. Afonso, J. Vale, E. Oliveira, F. Lau, and A. Suleman. A review on non-linear aeroelasticity of high aspect-ratio wings. *Progress in Aerospace Sciences*, 89:40–57, 2017.

[2] In Lee, Seung Ho Kim, and Hirokazu Miura. Static aeroelastic characteristics of a composite wing. *Journal of Aircraft*, 34(31):1413–1416, 2015.

[3] Maxwell Blair, Robert A. Canfield, and Ronald W. Roberts. Joined-wing aeroelastic design with geometric nonlinearity. *Journal of Aircraft*, 42(4):832–848, 2012.

[4] M. J. Patil and D. H. Hodges. On the importance of aerodynamic and structural geometrical nonlinearities in aeroelastic behavior of high-aspect-ratio wings. *Journal of Fluids and Structures*, 19(7):905–915, 2004.

[5] Mark Drela. Integrated simulation model for preliminary aerodynamic, structural, and control-law design of aircraft. In *Structures, Structural Dynamics, and Materials Conference and Exhibit*.

[6] M. J. Patil, D. H. Hodges, and C. E. S. Cesnik. Nonlinear aeroelasticity and flight dynamics of high-altitude long-endurance aircraft. *Journal of Aircraft*, 38(1):88–94, 2001.

[7] Zhang Jian. Static and dynamic characteristics of coupled nonlinear aeroelasticity and flight dynamics of flexible aircraft. *Acta Aeronautica Et Astronautica Sinica*, 32(9):1569–1582, 2011.

[8] Andrea Arena, Walter Lacarbonara, and Pier Giovanni Marzocca. Nonlinear aeroelastic formulation for flexible high-aspect ratio wings via geometrically exact approach. 2011.

[9] C. C. Xie, C. An, Y. Liu, and C. Yang. Static aeroelastic analysis including geometric nonlinearities based on reduced order model. *Chinese Journal of Aeronautics*, 30(2):638–650, 2017.

[10] C. C. Xie, L. B. Wang, C. Yang, and Y. Liu. Static aeroelastic analysis of very flexible wings based on non-planar vortex lattice method. *Chinese Journal of Aeronautics*, 26(3):514–521, 2013.

[11] G. Romeo, G. Frulla, E. Cestino, and G. Corsino. Heliplat: Design, aerodynamic, structural analysis of long-endurance solar-powered stratospheric platform. *Journal of Aircraft*, 41(6):1505–1520, 2004.

[12] I. Tuzcu, P. Marzocca, E. Cestino, G. Romeo, and G. Frulla. Stability and control of a high-altitude, long-endurance uav. *Journal of Guidance Control and Dynamics*, 30(3):713–721, 2007.

[13] M. A. Crisfield. A consistent corotational formulation for nonlinear, 3-dimensional, beam-elements. *Computer Methods in Applied Mechanics and Engineering*, 81(2):131–150, 1990.

[14] M. A. Crisfield, U. Galvanetto, and G. Jelenic. Dynamics of 3-d co-rotational beams. *Computational Mechanics*, 20(6):507–519, 1997.

[15] Joseph Katz and Allen Plotkin. *Low-Speed Aerodynamics, Second Edition*. Cambridge University Press.

[16] R. L. Harder and R. N. Desmarais. Interpolation using surface splines. *Journal of Aircraft*, 9(2):189–191, 2012.


## Contact Author Email Address

Mail to: zhangchi_npu@mail.nwpu.edu.cn

## Copyright Statement